DOE/BC/14994-8
OSTI ID: 9320

CT MEASUREMENTS OF TWO-PHASE FLOW IN FRACTURED POROUS MEDIA

SUPRI TR 104

By
Richard G. Hughes
William E. Brigham
Louis M. Castanier

June 1997

Work Performed Under Contract No. DE-FG22-96BC14994

Stanford University
Stanford, California

National Petroleum Technology Office
U. S. DEPARTMENT OF ENERGY
Tulsa, Oklahoma

DISCLAIMER

DOE/BC/14994-8
Distribution Category UC-122

CT Measurements of Two-Phase Flow in Fractured Porous Media

SUPRI TR 104

By
Richard G. Hughes
William E. Brigham
Louis M. Castanier

June 1997

Work Performed Under Contract DE-FG22-96BC14994

Prepared for
U.S. Department of Energy
Assistant Secretary for Fossil Energy

Thomas Reid, Project Manager
National Petroleum Technology Office
P.O. Box 3628
Tulsa, OK 74101

Prepared by
Stanford University
Petroleum Engineering Department
65 Green Earth Sciences Bldg.
Stanford, CA 94305

Contents

List of Tables

List of Figures

Abstract

The simulation of flow in naturally fractured reservoirs commonly divides the reservoir into two continua – the matrix system and the fracture system. Flow equations are written presuming that the primary flow between grid blocks occurs through the fracture system and that the primary fluid storage is in the matrix system. The dual porosity formulation of the equations assumes that there is no flow between matrix blocks while the dual permeability formulation allows fluid movement between matrix blocks. Since most of the fluid storage is contained in the matrix, recovery is dominated by the transfer of fluid from the matrix to the high conductivity fractures. The physical mechanisms influencing this transfer have been evaluated primarily through numerical studies. Relatively few experimental studies have investigated the transfer mechanisms. Early studies focused on the prediction of reservoir recoveries from the results of scaled experiments on single reservoir blocks. Recent experiments have investigated some of the mechanisms that are dominant in gravity drainage situations and in small block imbibition displacements. The mechanisms active in multiphase flow in fractured media need to be further illuminated, since some of the experimental results appear to be contradictory.

This report describes the design, construction, and preliminary results of an experiment that studies imbibition displacement in two fracture blocks. Multiphase (oil/water) displacements will be conducted at the same rate on three core configurations. The configurations are a compact core, a two-block system with a 1 mm spacer between the blocks, and

a two-block system with no spacer. The blocks are sealed in epoxy so that saturation measurements can be made throughout the displacement experiments using a Computed Tomography (CT) scanner.

Preliminary results are presented from a water/air experiment. These results suggest that it is incorrect to assume negligible capillary continuity between matrix blocks as is often done.

Acknowledgments

Financial support during the course of this work was provided by the Department of Energy through the Stanford University Petroleum Research Institute, under Contract No. DE-FG-22-93BC14899, and the SUPRI-A Industrial Affiliates.

Section 1

Introduction

One of the more difficult problems in petroleum, geothermal and environmental engineering is modeling the flow of fluids through naturally fractured porous media. Typically, for computational purposes, fractured media are broken into two continua. The matrix is considered to be that part of the medium which contains the majority of the solid rock. This portion is assumed to have most of the fluid storage capacity of the system, but little conductivity. The fractures are considered to be an interconnected network of high conductivity channels. The fractures are assumed to have negligible storage capacity.

In a dual porosity formulation of the problem, transport between matrix blocks is not allowed. The system of fractures is rapidly drained due to the high conductivity. Transfer of the matrix fluid to the fracture system is through the pressure difference between the systems in the area around each matrix block.

A dual permeability formulation of the fractured flow problem allows the transfer of fluids from one matrix block to another as well as the transfer from matrix blocks to the fracture system. The finite difference form of the dual permeability formulation is given by Kazemi, (1990):

Fracture Equation:

$$\Delta \left[T_{pf} \left(\Delta p_{pf} - \gamma_{pf} \Delta D_f\right)\right] - \tau_{pmf} + q_{pf} = \frac{V}{\Delta t} \Delta_t \left(\frac{\phi S}{B}\right)_{pf} \tag{1.1}$$

Where:

T_{pf} = the transmissibility of phase p in the fracture system
Δp_{pf} = the change in the phase pressure between grid blocks in the fracture system for phase p
γ_{pf} = the density of phase p in the fracture system
ΔD_f = the change in the depth between grid blocks in the fracture system
τ_{pmf} = the matrix–fracture transfer function for phase p
q_{pf} = source term for phase p in the fracture system
V = the grid block volume
Δt = the time step size for the simulation
$\Delta_t \left(\frac{\phi S}{B}\right)_{pf}$ = the change over the time step of the porosity, phase saturation, and formation volume factor of phase p for the fracture system

Matrix Equation:

$$\Delta \left[T_{pm} \left(\Delta p_{pm} - \gamma_{pm} \Delta D_m\right)\right] + \tau_{pmf} + q_{pm} = \frac{V}{\Delta t} \Delta_t \left(\frac{\phi S}{B}\right)_{pm} \tag{1.2}$$

All terms are as defined in the fracture equations with the subscript "m" signifying a matrix property, replacing the subscript "f" which signifies a fracture property. The transmissibility terms are given by:

$$T_{pf} = \frac{A\phi}{L} k_f \left(\frac{k_r}{\mu B}\right)_{pf} \tag{1.3}$$

$$T_{pm} = \frac{A\phi}{L} k_m \left(\frac{k_r}{\mu B}\right)_{pm} \tag{1.4}$$

Where the new term definitions are:

A = the grid block area in the direction of flow
L = the grid block length in the direction of flow
k_f = the grid block permeability of the fracture system
k_m = the grid block permeability of the matrix system
k_r = the grid block relative permeability of phase p
μ = the viscosity of phase p

The matrix-fracture interaction is modeled as a source function given by:

$$\tau_p = \sigma V k_m \left(\frac{k_r}{\mu B}\right)_{pmf} [p_{pf} - p_{pm} - \gamma_p (D_f - D_m)] \tag{1.5}$$

Where σ is the shape factor and has dimensions of $1/L^2$, V is the grid block volume and D_f and D_m are the fracture and matrix depths.

Note that for the dual porosity formulation of these equations, the T_{pm} term is set to 0 and, for grid blocks with no source terms, the matrix-fracture transfer function in the matrix equation simplifies to:

$$\tau_p = \frac{V}{\Delta t} \Delta_t \left(\frac{\phi S}{B}\right)_{pm} \tag{1.6}$$

The objective of this study is to obtain additional data on the physical mechanisms that effect the flow of fluids in these dual systems. The motivation to collect this information lies in the uncertainty associated with many of the primary variables both in the transfer function and in the general equations. As will be shown in Section 2, much of the early work on dual systems assumed that the fracture capillary pressure was negligible and that fracture relative permeability was equal to the phase saturation. Recent research on these systems has concentrated on modifying the matrix-fracture transfer functions to better account for the capillary, viscous, and gravitational forces present in real fractured media. Much of this work has been numerical matching of the sparse experimental data that exists in the literature,

however, there is a dilemma. Many of the experimental researchers have commented that some of their results are either contradictory to, or difficult to explain with existing theory. Part of the problem lies in the lack of information on how the fluids are moving in the experiments.

By contrast, the work reported here tracks the movement of the phases with a Computed Tomographic (CT) scanner. It can also include detailed rate and pressure measurements throughout the experiment. The experimental setup is detailed in Section 3. As this is the first stage in the development of this experimental process, only preliminary experimental results are presented in Section 4. Finally, some discussion of the results and recommendations for further work in this area are presented in Section 5.

Section 2

Literature Review

Knowledge advancement in the area of two-phase flow in fractured porous media has largely been done through numerical simulation studies. Numerical researchers perform fine grid simulations to determine the relative effects of various parameters to come up with better ways to represent the physical flow processes in dual porosity simulators. Usually these studies have returned to the sparse experimental data in the literature to verify their models. This section will review the references most commonly cited as well as some of the other experimental work done in support of the dual porosity/dual permeability formulation of fractured systems. This discussion concentrates on answering the questions "what was done" and "what results were presented" (as opposed to "what did the authors conclude").

2.1 Graham and Richardson (1950)

Graham and Richardson (1950) used a single block of fused quartz in their experiments. The block was in the shape of a right isosceles triangle. The sides with equal length were 1 foot long and 1.5 inches thick. Permeability of the block was 27 Darcies and porosity was 45%. The block was sealed with plastic coating except on the two equal length sides which represented the fracture faces. Stainless steel bars were fitted to the fracture faces and positioning screws allowed the bars to simulate fracture widths from 0 to 0.05 inches. Fluid entry and exit ports were located in the

space between the stainless steel bars and the fracture faces adjacent to the two ends of the long side of the triangle. Distilled water and kerosene were the fluids used in the experiments. Pressure drop across the experiment and oil and water production were measured for various configurations of fracture width and water injection rates. The experiments were terminated when oil production had "almost ceased." Then flooding was stopped, the fracture was closed and the model was weighed. Injection rates reported were from 1.15 cm^3/sec to 6.31 cm^3/sec.

Reported results were graphs of water-oil ratio (WOR) versus (vs) water saturation (S_w) for a constant fracture size at various injection rates and WOR vs S_w for a constant injection rate at various fracture widths. The authors also used scaling procedures to determine reservoir-scale production estimates from their experiments. They provided graphs of oil rate vs injection rate and WOR vs S_w for these estimates.

These researchers found that oil production from their model was rate sensitive (higher injection rates required more water to recover a given amount of oil). They also found that increasing the fracture/matrix permeability ratio by increasing the fracture width caused an increase in the amount of water required to recover oil from the block; however, this increase was less than proportional to the increase in fracture width.

2.2 Mattax and Kyte (1962)

Mattax and Kyte (1962) derived a scaling law to allow the use of imbibition tests performed on small reservoir core samples to predict field performance during imbibition dominated waterfloods. To verify their derivation, the authors performed several experiments.

Linear experiments were performed where cylindrical alundum samples of various lengths and permeabilities were encased in plastic with a single, flat face left open. The samples were saturated with oil, and then immersed in water, allowing water to imbibe into the sample through the open face. Three dimensional (3D) experiments were also conducted. Cylindrical Weiler sandstone cores of various sizes were used for these experiments. The cores were saturated with oil and then immersed in water

as in the linear tests, but the cores were not encased in plastic. For all of these experiments, plots of oil recovery vs time were presented. Additionally, all of the results were plotted on a graph of oil recovery vs the derived dimensionless scaling parameter,

$$t_D = t\sqrt{\frac{k}{\phi}}\frac{\sigma}{\mu_w L^2} \tag{2.1}$$

Where:

t = the displacement time
k = absolute permeability
ϕ = porosity
σ = interfacial tension
μ_w = water viscosity
L = the characteristic dimension of the sample

Another sequence of experiments was performed using a 3 inch cubical sample of a reservoir core (origin of the core was not given). The core was placed in a transparent vessel that was filled with oil with clearance on all sides (the core sat on stilts to provide the clearance on the bottom). The core was initially at connate water saturation. Water was introduced from below at constant rates. Oil was allowed to flow out of a port near the top of the vessel. When the water had passed the top of the core, the water level was maintained at a constant height above the top of the core until no further oil was recovered. The critical rate of water advance was defined as the rate at which the oil recovery was below the maximum oil recovery from a series of experiments on the same sample at different water advance rates.

The last sequence of experiments involved taking two strongly water-wet cores and encasing each in plastic with one open face as in the first set of experiments. These two cores were then clamped together with open faces separated by metallic spacers. The cores, initially at connate water saturation, were then immersed in water and oil recovery vs time was noted. Various spacer sizes were used to evaluate the effect of fracture width on recovery. Fracture widths greater than 25 μm produced identical

recovery curves. An experiment conducted with a spacer size of 10 μm provided the same cumulative recovery but the rate of the recovery was much slower.

Scaling of this experimental data has been done by other authors. Using a form proposed by Aronofsky et al (1958), De Swaan (1978) presented a comparison between the data from one of the 3D immersion experiments and the equation:

$$r = R\left(1 - e^{-\lambda t}\right) \tag{2.2}$$

Where:

r = the recovery at time, t
R = the limit toward which recovery converges
λ = a constant giving the rate of convergence to R

The lambda value that was found to match the data was 2.7.

Kazemi et al (1992) were able to scale the data for all of the experiments without spacers into the form:

$$r = R\left(1 - e^{-\lambda_D t_D}\right) \tag{2.3}$$

The t_D and λ_D terms are given by the following expressions:

$$t_D = \left[\sqrt{\frac{k}{\phi}}\left(\frac{\sigma F_s}{\mu_w}\right)\right] \cdot t \tag{2.4}$$

$$\lambda_D = \left[\sqrt{\frac{\phi}{k}}\left(\frac{\mu_w}{\sigma F_s}\right)\right] \cdot \lambda \tag{2.5}$$

F_s is the matrix block shape factor and was defined as:

$$F_s = \frac{1}{V_{ma}} \cdot \sum_s \frac{A_{ma}}{d_{ma}} \tag{2.6}$$

Where:

V_{ma} = the volume of the matrix block
A_{ma} = the area of a surface open to flow in a given flow direction
d_{ma} = the distance from the open surface to the center of the matrix block

The sum is taken over all the open surfaces of the matrix blocks.

No mention is made in either of these scaling studies of the experimental data with the spacers, although Kazemi et al (1992) suggest that in Eq. 2.2, λ is a constant that is equal to the reciprocal of the time required to recover 63% of the recoverable oil. This scaling does seem to hold for the experiments with spacers.

2.3 Parsons and Chaney (1966)

Parsons and Chaney (1966) used outcrop and subsurface samples of the Madison formation in Wyoming for their experiments. These carbonate samples were made water wet either by heat treatment or by solvent cleaning. It was noted that heat treating produced stronger imbibition characteristics than solvent cleaning. The oil phase was a white mineral oil and distilled water was the displacing fluid. Two types of experiments were conducted. The first was an immersion experiment where an oil saturated sample was submerged in a water bath. Submerged weight was recorded vs time. Blocks measuring 2 × 2 × 1 inch were tested initially. These blocks were then split into four 1 × 1 × 1 inch cubes and retested. Pore volumes of oil recovered vs the Mattax and Kyte (1962) dimensionless scaling parameter (Eq. 2.1) were presented. The plots for each of the tests did not overlay one another. The authors suggest that this was due to the heterogeneity of the rock. This suggestion could have been evaluated by summing the results of the small block experiments and dividing by the number of blocks, but was not reported.

The second type of experiment used either 1 × 1 × 12 inch or 4 × 4 × 12 inch blocks of the rock samples. In these experiments, an oil saturated sample was placed

into a Plexiglas cell that was inside a constant temperature cabinet. The cell for the one inch sample had a 1/8 inch clearance between the cell and the rock, and the cell for the four inch samples had a 1/4 inch clearance between the cell and the rock. The space between the cell and the sample was filled with oil. A constant water head inlet tube was connected to the bottom of the cell. The outlet at the top of the cell was connected by tubing to a collection beaker that was also inside the constant temperature cabinet. The height of the outlet tubing could be adjusted by a motorized pulley system connected to the collection beaker.

The experiments began by adjusting the height of the outlet tubing such that water was allowed into the Plexiglas cell to a level just below the bottom of the rock sample. The oil-water interface inside the cell was then allowed to rise at a predetermined rate by lowering the outlet tubing. The height of the oil-water interface, the volume of oil displaced and the height of the outlet tubing were noted as functions of time.

In some of the experiments a zone of discoloration advanced ahead of the oil-water interface. The authors felt that this discoloration zone was due to water imbibing ahead of the oil-water interface. When this zone occurred, its height was also noted. The experiments terminated after the oil-water interface passed the top of the sample and after oil production had stopped.

Graphs were presented on the heights of the oil-water interface vs elapsed time and the heights of the oil-water interface vs oil recovery. The data suggest that higher rates of rise in the oil-water interface produce lower recovery rates. Part of the difficulty in interpreting the results of these experiments is that the reported rates of rise were measured late in the experiment. The confusion lies in the fact that on one of the graphs of height vs time, the highest of the reported rates of rise takes the second longest time to reach the top of the cell.

In these experiments, it was also noted that the size and shape of the zone of discoloration varied greatly. In some experiments the zone was uniform and piston-like, while in others the zone was highly irregular.

2.4 Kyte (1970)

Kyte (1970) noted that in cases where gravity segregation is as important as imbibition, experiments performed in a centrifuge can be used to predict recoveries. The procedure that was suggested was to obtain a preserved core and cut a sample from the core to simulate the reservoir matrix block geometry. The sample should then be saturated with oil and connate water. The sample can then be placed into a centrifuge cup containing the displacement water, and centrifuge experiments can be conducted at speeds which are derived through scaling arguments.

Cylindrical cores 1.88 cm diameter × 4.9 cm length and 3.76 cm diameter × 9.8 cm length were used for these experiments (origin of the cores was not given). The results of the experiments were scaled to a reservoir whose matrix blocks were 69.8 cm diameter × 1.82 m in length. The scaled results, with experimental scatter, agreed with the theory the author derived. He also scaled some immersion experiments and showed that recoveries, with gravity considered, were considerably higher than recoveries for imbibition alone.

2.5 Iffly et al (1972)

Iffly et al (1972) performed experiments on a variety of reservoir samples from an unnamed ELF field. Some of the samples were consolidated cores but most were unconsolidated. The samples were described as a clayey silt with porosities ranging from 10 to 35%, and with permeabilities ranging from 30 to 2000 md. Each sample had a different mix of primary constituents: carbonate, clay, and silica. The samples were placed in a tube apparatus which allowed a variety of inlet and outlet boundary conditions to be tested.

The boundary conditions tested were water at constant potential above and below the sample (Type A tests), water on the bottom surface of the sample with a no flow boundary on the top surface of the sample (Type B tests), water on the top surface of the sample with a no flow boundary on the bottom surface of the sample (Type C tests), water on the top surface of the sample with oil on the bottom surface of the

sample (Type D tests), and water on the bottom surface of the sample with oil on the top surface of the sample (Type E tests). Type E tests proved to be the most favorable configuration for recovery of oil from the system, while Type B tests proved to be the most unfavorable configuration.

Reservoir oil, reservoir water, and sea water from near the field were used for most of the experiments, since it was found that using substitute fluids caused results that were significantly different from what would be predicted from scaling laws. The authors attributed this discrepancy to smaller interfacial tension decline rates with field fluids compared to rates with substitute fluids. This was a qualitative observation found by mixing the fluids in a closed tester. Phase segregation occurred faster in the actual fluids than in the artificial fluids. Once the phases were segregated, surface tension of the water phase was measured. The surface tensions of the field waters were greater than the surface tensions of the artificial waters.

Experimental results were presented as normalized recovery (N_p/N) vs reduced time. This reduced time was defined as:

$$\bar{t} = t \cdot \frac{\sigma \cos\theta}{\mu_o h^2} \sqrt{\frac{k}{\phi}} \tag{2.7}$$

Where:

t = the displacement time
k = absolute permeability
ϕ = porosity
σ = interfacial tension
μ_o = oil viscosity
h = sample thickness
θ = the oil/water contact angle

Note the similarity to Eq. 2.1. Since the characteristic dimension for these experiments is h, the two equations differ only in the viscosity term and in the treatment of the contact angle.

Three of the experimental results were matched with a simulator. One experiment required an adjustment to the upper portion of the capillary pressure curve to match. The other two experiments required an increase in the curvature of the oil relative permeability curve in addition to the capillary pressure curve adjustment to obtain a match. One of the tests had a graph of saturations measured by gammagraphy and one sample had saturations reported that were determined by solvent extraction.

Three primary conclusions from this work were: lithology matters in predicting recovery from fractured media (samples with high carbonate content showed lower recoveries), using substitute fluids can result in erroneous predictions of recovery, and contaminated fluids or poorly chosen chemical treatments for field fluids can have an adverse effect on recovery. Additionally, this research showed that boundary conditions for the blocks must be considered. When gravity forces are aligned to aid imbibition, recoveries can be greatly increased.

2.6 Kleppe and Morse (1974)

In support of the construction of a numerical model for simulating flow in fractured systems, Kleppe and Morse (1974) performed flow experiments similar to those by Mattax and Kyte (1962). A four foot long, four inch diameter, cylindrical Berea sandstone core was placed in a Plexiglas tube with a 2.5 mm annular space between the core and the tube. Narrow strips of conductive paint were applied directly to the core to measure saturations through resistivity measurements. Brine and kerosene were the fluids used in the experiments. The core was evacuated, saturated with brine, flooded with kerosene until the oil-water ratio (OWR) exceeded 100, and placed in the Plexiglas tube filled with kerosene. Brine was injected into a port at the bottom of the tube and displaced fluid was allowed to leave through a port, open to the atmosphere, at the top of the tube. Cumulative oil and water production and height of the oil/water interface were recorded as functions of time. The experiments terminated when the WOR exceeded 30.

The authors found that, at low injection rates, the displacement of oil from the core was "almost piston-like." Essentially no oil was produced after the water level

was at the top of the core. At high rates, water breaks through earlier, but oil production continues after the interface has reached the outlet. The definition of low and high rates was not given in the paper, but Beckner (1990) says that the low rate reported in this work was 3.3 cm^3/min, while the high rate was 35 cm^3/min.

2.7 Lefebvre du Prey (1978)

Two types of experiments were conducted by Lefebvre du Prey (1978). The first was the imbibition displacement of oil by water in the presence of additional gravitational forces exerted by the use of a centrifuge much like the experiments by Kyte (1970). Various block dimensions were used to test scaling rules. Fountainebleau sandstone was the rock used, fluid phases were distilled water and a 50-50 mixture of Bayol 50 paraffin oil and aromatic free kerosene.

Results were presented as recovery plots vs a dimensionless time. The dimensionless time was either scaled with respect to capillarity or with respect to gravity. These scaling arguments were defined by the author as:

Capillary Scaling

$$t_{Dc} = t \cdot \frac{P_{ct} \cdot (k_o)_{max}}{h^2 \cdot \phi \cdot \Delta S \cdot \mu_o} \tag{2.8}$$

Gravity Scaling

$$t_{Dg} = t \cdot \frac{\Delta\rho \cdot g \cdot (k_o)_{max}}{h \cdot \phi \cdot \Delta S \cdot \mu_o} \tag{2.9}$$

Where:

$(k_o)_{max}$ = maximum effective permeability to oil
ΔS = change in saturation
P_{ct} = displacement pressure at the time of the first oil recovery
$\Delta\rho$ = density difference
g = acceleration of gravity

Scaled recovery curves were also presented. These scaled curves were for an assumed set of reservoir scale block parameters. Permeability, porosity, initial saturation, and "displacement pressure at the time of the first oil recovery" (P_{ct}) were defined as constants for the reservoir scale blocks, and the reservoir scale block height was calculated from the gravitational forces placed on the experimental block in the centrifuge. The author concludes from these experiments that scaling small sample recovery data to predict reservoir recoveries warrants further study, due to the deviation of his results from theory.

The second type of experiment performed used parallelepiped Fountainebleau sandstone blocks that were sealed on all but one large face. The open face was placed opposite a glass plate that was attached to the block to serve as the fracture (no mention is made as to how the plate was attached to the block nor the width of the opening that was created between the plate and the open block face). The blocks were initially saturated with oil (a variety of oil phases were used). Water was then injected into the bottom of the fracture with outflow at the top of the fracture. Fluid flow in the fracture was observed visually and several of the experiments had saturation measurements made by gamma-ray absorption.

The author presented one figure that attempted to show the seemingly random manner with which oil evolved from the blocks. An additional figure showed several saturation maps from gamma-ray absorption of one of the experiments. When injection rates were small, the author reported that water entered the lower portion of the block, moved to the center of the block and then migrated in all directions. At high rates, the water reportedly entered the block in a front across the surface of the fracture. The water slowly advanced laterally into the block.

2.8 Kazemi and Merrill (1979)

The work by Kazemi and Merrill (1979) was performed on Berea sandstone cores. Both cylindrical cores and rectangular block cores were used in the experiments. The cylindrical cores were one inch in diameter and three inches in length. The rectangular blocks were either four inches tall, two inches wide, and four inches in

length or the blocks were two inches tall, two inches wide, and four inches in length. One experiment was conducted on an unfractured, cylindrical core. The rest of the experiments were conducted on cores that were cut in half, lengthwise and glued back together with epoxy with no spacers between the halves.

For the fractured systems, injection and production were constrained to the fractures. For the cylindrical cores, this was accomplished by the construction of a rubber end piece with a hole cut in the center. For the rectangular blocks, a piece of tubing had a channel cut on one side. A piece of this tubing was then glued with epoxy to each end face at the fracture. The remainder of the block was then sealed with epoxy. The injection line was connected to the tubing with the channel. A similar connection was made to the production end. The only mention made of the fluid distribution system for the unfractured core was that a Hassler core holder was used.

A 2000 ppm NaCl solution was the aqueous phase used and either diesel fuel or n-decane was used as the oil phase. In all but one test, the cores were initially saturated with the oil phase and brine was injected at various rates. That one test had an initial brine saturation of 43%.

Results of these experiments were presented through graphs of pore volume (PV) oil recovered vs PV water injected and water-oil ratio vs PV water injected. Low rate ($\sim$ 1 cm^3/hr) injection performed in an expected manner. When rates were increased to around 6 cm^3/hr, breakthrough was immediate. Water-oil ratio was initially high ($\sim$ 2-3), then fell to approximately one and stabilized. After an additional 0.5 PV of water had been injected, the WOR began rising in an exponential fashion, which was similar to the climb at breakthrough in the low rate experiments. The immediate breakthrough in the higher rate experiment did not occur in the experiment run with an initial water saturation.

2.9 Horie et al (1988)

Horie et al (1988) performed stacked block experiments using cylindrical Berea sandstone cores that were approximately 10 cm in diameter and 30 cm in length. Three of these cores were stacked vertically and placed into a transparent core holder. The

cores were stacked face-to-face either with, or without, spacers between the blocks. Three different configurations were used for the spacers. The first configuration was to use four square aluminum shims that were 0.012 in. thick. The second used coarse sand grains approximately 0.014–0.017 in. in diameter. These sand grains were sparsely distributed in the space between the blocks. The third configuration used fine (0.0059–0.0083 in. diameter) sand grains that covered the space between the blocks with a single layer. The fine sand grains were said to be about the same size as the grains of the Berea sandstone.

N-decane was the oil phase used and air was used as the displacing fluid. The blocks were saturated with the n-decane and were stacked in a core holder that was filled with oil. The oil was allowed to drain out of the holder until the space between the core holder and the blocks was produced. Once this occurred, production vs time was recorded. When the oil production rate had "nearly ceased," an overburden pressure was applied to the stacked blocks. After the experiments terminated, the blocks were weighed to determine the block saturations. The authors noted that the oil that was produced from their experiments did not flow along the vertical space between the blocks and the core holder. The supposition was that the oil flowed out the lower block. The authors also suggested that oil was flowing across the fractures and was reinfiltrating the lower blocks.

Results from this work suggest that capillary continuity between the blocks has a significant effect on total recovery. Only about 3% of the pore volume was produced for the case where the aluminum spacers were used, whereas 23% of the pore volume was produced when the blocks were in direct contact with no overburden. In the experiment where the blocks were separated by the aluminum spacers, no additional recovery was obtained upon addition of the overburden pressure. The use of the fine grained sand as a spacer resulted in approximately 17% PV recovery before application of the overburden pressure, and recovery increased to 23% once the overburden pressure was added.

The coarse grained sand spacer experiment was even more interesting. This experiment had a recovery that was a bit more than the aluminum spacer test before the application of the overburden pressure (about 3.5% recovery), but increased to

23% once the overburden pressure was applied. Note that this was the same as the result with other spacer configurations. Once the experiment was terminated it was noted that the coarse sand grains had been crushed due to the overburden.

2.10 Firoozabadi and Hauge (1990)

Firoozabadi and Hauge proposed modeling fracture capillary pressure by assuming that the fracture faces are made up of a sequence of cones. They assumed that the apex of a cone on one side of the fracture face touches the apex of a cone on the adjacent face. To support their model, mineral oil/air experiments were conducted in a centrifuge on rock samples from a chalk outcrop from Denmark. A single cylindrical block experiment was run on a rock sample by placing a mineral oil saturated sample into a core holder with spacers on the bottom and on the sides. Once the single block experiment was completed, it was cut into several different block configurations which are described in detail by the authors. These blocks were then stacked and placed into the core holder with the same spacer configuration between the blocks and the core holder as in the single block experiment. No spacer was placed between the blocks. The experiments were run at 2036 rpm. The volume of drained liquid was recorded vs time and, upon completion of the experiments, block saturations were measured by weighing the blocks.

The results of these experiments again indicate that capillary continuity is a significant factor in the recovery of oil from stacked blocks. In general, it was found that the more blocks that are stacked, the lower the recovery. In one of the experiments the results could not be correlated to known mechanisms and were attributed to a "more complicated flow process than the reimbibition mechanism" that was assumed. With the exception of the one case, the results showed agreement with their model.

2.11 Labastie (1990)

Labastie used two 35 cm homogeneous sintered ceramic matrix blocks with 5 mm spacers made of differing materials to study capillary continuity in gravity drainage

experiments. The matrix blocks had high permeability (4.6 Darcies) and high porosity (44%). The experiments were performed with spacers that had the same permeability as the matrix blocks, spacers that had a much smaller permeability (5 md), and spacers that had no permeability (either stainless steel or glass beads). The block faces had an area of 45.36 cm^2 and the spacers occupied approximately 16.7% of the block face area. The oil phase was ISOPAR M and air was the gas phase used in the experiments.

Experimental results were presented in recovery vs time curves. The 4.6 Darcy bridge showed significantly higher recoveries in a shorter time than the other types of spacers. The 5 md spacer provided the next highest recovery curve. The glass bead spacer and the stainless steel spacer had almost the same recovery curves; however, it should be noted that the stainless steel spacer size was actually 0.3 mm, rather than the 5 mm size for the glass beads. The 5 mm stainless steel spacer experiment provided no recovery. Labastie suggested that one reason for the lack of recovery may have been that the spacers may not have provided a clean contact on either of the matrix block faces. Contact area then may have been too small to provide the necessary capillary continuity. An additional possibility for explaining the poor performance of the square spacers could be that the contact was clean, but that flow was in a thin film along the spacer. The area available for flow would be limited to a thin square shell around the spacer.

2.12 Firoozabadi and Markeset (1992a, 1992b)

In a series of papers, Firoozabadi and Markeset (1992a, 1992b) extended the stacked block work of Horie et al (1990). The first sequence of experiments (Firoozabadi and Markeset, 1992b) was to show the effects of block height on recovery. Experiments were run on a stack of four Berea sandstone blocks that were 45.5 cm tall and on a stack of three Berea blocks that were 60.5 cm tall. The 45.5 cm experiments were run with six configurations of metallic spacers separating the blocks. These configurations were: no spacers between the blocks; three, 1.2 mm spacers between the blocks; three, 0.25 mm spacers; 49, 0.25 mm spacers; five, 0.1 mm spacers; and nine, 0.1 mm spacers.

The 60.5 cm experiments also had several spacer configurations. These were: four, 50 μm spacers between the blocks; 16, 50 μm spacers; and a configuration that consisted of four, 100 μm spacers for 3 weeks; four 50 μm spacers for four weeks; and blocks in direct contact for a week and a half. Results were presented in semi-log plots of cumulative production vs time and log-log plots of production rate vs time. Block saturations, obtained by weighing, were also presented.

These experiments showed that stacked blocks in direct contact produced the same recovery as an equal height single block experiment. Additionally, the experiments showed a marked reduction in recovery depending on spacer size and number of spacers. The more even the fracture width for a given spacer size, the lower the recovery. This led the authors to conclude that fracture-liquid transmissibility may not be strongly influenced by contact area or the number of contact points, but is strongly influenced by fracture aperture. These authors also feel that the fracture-liquid flow in gas/oil gravity processes occurs mainly by film flow.

The second sequence (Firoozabadi and Markeset, 1992a) was to show the effects of capillary and gravity crossflow. This work started with stacked block experiments where the stack could be tilted at various angles. Two such experiments were conducted. The first used four, 0.25 mm metallic spacers between the blocks and the blocks were tilted at a 30° angle from vertical. The second used no spacers between the blocks with a tilt angle of 45°.

The next phase was to run similar experiments with a matrix of stacked slabs. The matrix consisted of four rows of three slabs each. Unlike the previous experiments, the stacked slab experiments were run with the outer faces in direct contact with the walls of the core holder. No spacers were used between the slabs or the rows. Tilt angles were 0°, 30°, and 45° from vertical.

This work showed that gravitational effects can dramatically alter recoveries and that capillary crossflow can enhance recoveries. When compared to the vertical stack results, the 30° tilt caused a 33% reduction in recovery for a given time, and the direct contact, 45 ° angle, data showed more than a factor of three increase in the amount of time required to recover equal volumes of oil. A comparison of the stacked block experiment at a 45° angle with the stacked slabs at a 45 ° angle indicates that

the stacked slab configuration recovered approximately the same amount of oil as the stacked block configuration in 20% less time.

2.13 Babadagli and Ershaghi (1992)

Three rock types were used in this work. Two low permeability rocks, Colton Sandstone (k = 0.05-0.1 md) and Austin Chalk (k = 3-4 md), and one higher permeability rock, Berea Sandstone (k = 280-300 md). Cylindrical core samples one inch in diameter and four inches in length were used. Some of the experiments were run on cores that were cut into two hemispherical pieces that were held together by epoxy and heat shrinkable Teflon with no spacers between the halves. Other experiments were run on cores cut into hemispheres and further subdivided lengthwise into one inch pieces. The eight resulting pieces were then held together with epoxy and the heat shrinkable Teflon. After cutting, the samples were placed either into a Hassler sleeve equipped core holder, or into a core holder that was constructed of a plastic acrylic tube with end plugs that directed the flow into the core. The samples were then saturated with kerosene. A 3% KCl solution was the displacing fluid. The experiments using the acrylic tube core holder used a CT scanner to determine water front locations with time. Some of the experiments on the four inch long samples were run in the vertical direction.

Results were presented in plots of PV recovery vs time, PV oil produced vs PV water injected, and water-oil ratio vs PV oil produced. Five schematics were also presented from the CT scans of water front position at various pore volumes injected. These results indicated that breakthrough times are highly rate dependent, even at very low injection rates. For all of the cases presented, breakthrough occurred earlier for increasing flow rates; consequently recovery of equivalent volumes of oil required more injected water. For the tighter samples, higher rates decreased ultimate recovery once a threshold injection rate was surpassed. For the very tight Colton sandstone experiments, oil recovery was only 10% of the pore volume and occurred almost immediately after injection at a rate of only 0.75 cm^3/min.

CT information indicated that for lower rates (0.2 cm^3/min), displacement progressed in the matrix faster than in the fracture. At a higher rate of 1 cm^3/min, the displacement advances rapidly through the fracture. In two of the cases shown, the water appeared to be advancing faster into the upper blocks than the lower blocks. One of the figures was for a displacement experiment run vertically. Water was injected into the bottom of the core holder with production out the top. This figure indicated that the water front moved much more rapidly in the matrix than in the fracture.

2.14 Summary

As the discussion above indicates, a more fundamental study of two-phase flow in fractured media is needed. One of the primary drawbacks to many of the experiments is the lack of understanding of the saturation distributions in the rock matrices.

Work sponsored under this program (Guzman and Aziz, 1993) was initiated to study two-phase flow in fractured porous media. The initial purpose for this work was to attempt to measure relative permeabilities in the fracture. An experiment was designed to measure saturation distribution in two cores of identical material. One core would be a control while the other would be cut in half and propped open with inert material to simulate a fracture. Oil and water would be injected into the cores at varying rates. Saturations would be measured by CT scanning the core at various stages of the injection process. Fine grid simulations would then be used to history match the experimental results. Fine grid simulations were performed to help in the design of the experimental procedure (Guzman and Aziz, 1991).

An experiment was built but, unfortunately, problems which developed during single phase injection testing, precluded obtaining results. The work reported here is a modification and extension of the Guzman and Aziz study. The focus will be on obtaining both qualitative and quantitative data on the movement of fluids in fractured blocks.

Section 3

Core Holder and Flow Equipment Construction

Three rectangular blocks of Boise sandstone were prepared for use in this work. The first is a compact (solid) core measuring 3 1/8 × 3 1/16 × 11 inches. The second and third cores are constructed from two 2 15/16 × 1 1/2 × 11 inch blocks. The second core system has a 1 mm thick spacer fastened in place with Epoxy 907 to provide a separation between the blocks to simulate a fracture. The third core system is constructed similarly but has no spacer between the blocks. The following sections will describe the materials and methods used to build the core holders and flow system for these experiments.

3.1 Core Holder

Due to the rectangular shape and the desire to measure in-situ saturations through the use of the CT scanner, conventional core holders could not be used. A core holder similar to the original design by Guzman (Guzman and Aziz, 1993) was developed for each of the cores. It consists of an epoxy resin surrounding the core. The resin system used was Tap Plastics Marine Grade Resin #314 with Tap Plastics #143 Hardener. Plexiglas end plates were constructed for the core holders with a piece of 3/8 inch Viton acting as a gasket surrounding the core and held in place with automotive

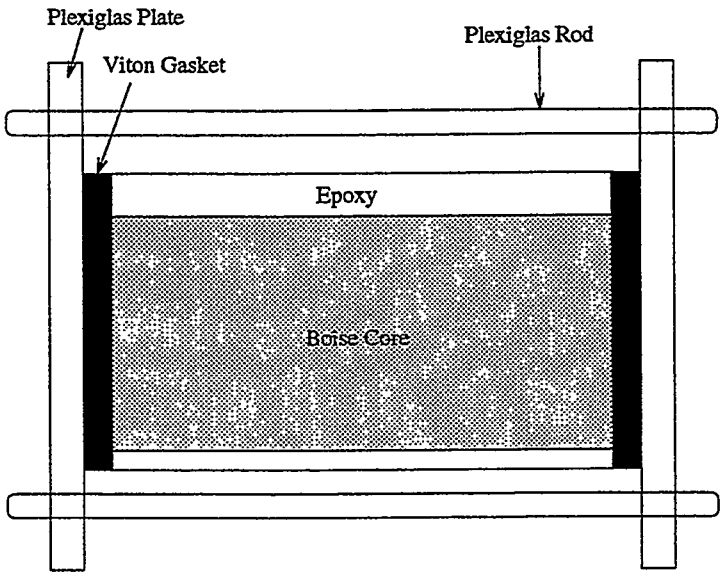

Figure 3.1: The Core Holder.

gasket material (Permatex Ultra Blue RTV Silicone Gasket) and Plexiglas rods as shown in Fig. 3.1.

The original design had six pressure taps all on the top of the core holder. The new design has two pressure taps on the top and two on the bottom. In addition, a Plexiglas plate that was epoxied to the top surface of the core was removed in the new design. The plate was found to be unnecessary and a potential source for leaks.

Several different epoxy systems were tested in addition to the system chosen. Among these were Tap Plastics 'One to One' General Purpose Epoxy, Tap Plastics 'Super Hard' Four to One Epoxy, and Evercoat Laminating Resin. All of these epoxies were extremely exothermic when reacting to become solid. The Tap Plastics Marine Grade Epoxy system selected uses the #314 resin in combination with various hardeners to provide different cure times with similar chemical resistances and strengths. The #143 Hardener was chosen because it provides a slower cure, yet retains its chemical resistance properties. This system is slightly less viscous so penetration is a bit deeper into the core than it was for some of the other systems we observed; however, for this experiment the added control the slow cure time provided was deemed to be a more important issue than penetration depth. Specifications for the epoxy system

chosen are given in Appendix A.

In addition to using a slower curing epoxy system, an aluminum mold was constructed to allow better heat dissipation. The mold was built so that there would be a 1/2 inch border of epoxy around the bottom and sides of the core. It had an open top with sides which were six inches taller than the estimated top of the epoxy. This allowed the heat to radiate out of the mold and helped to prevent cracking of the epoxy.

To construct the core holders, Plexiglas end plates were attached to the core with GE White RTV 102 Silicon Rubber Adhesive Sealant and held in place with clamps. Epoxy was layered on with a paintbrush and allowed to sit for one hour. The core was then placed into the mold. The mold was tilted at a 45 degree angle and the epoxy was poured in. Tilting the mold reduced the number of air bubbles which can form along the bottom of the core. Once the liquid resin covered the core, the mold was returned to level and additional resin was added to reach the desired height. During the construction of the compact core holder, heat expansion of the air inside the core caused air bubbles to form and rise to the surface of the epoxy at one of the ends. For the two subsequent cores, holes were drilled in the Plexiglas end plates. This action alleviated the problem. Figure 3.2 shows an oblique view of the core holder after the epoxy has cured.

Once the epoxy had cured, the cores were removed from the mold and taken to Donohoe and Carroll Memorials in Colma, CA where the ends were trimmed with a water-cooled diamond circular saw to provide an 11 inch length. A piece of 3/8 inch Viton was then cut for each end face of the core holder. A hole was cut in the Viton so that the core face would be exposed. Automotive gasket material was then used to glue the Viton to the epoxy and the Viton to the Plexiglas end plates. Plexiglas rods were bolted into place through holes that had been drilled into each end plate. This provided added support and also allowed the gasket material/Viton to be compressed to eliminate leaks.

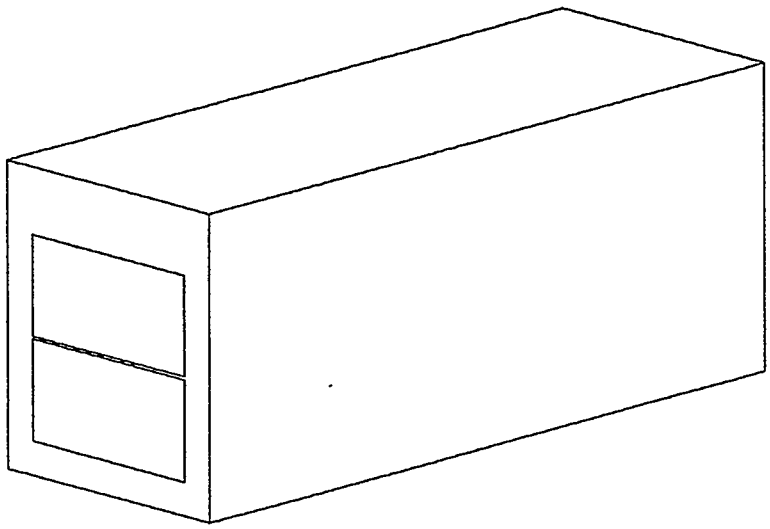

Figure 3.2: Core Holder After Curing.

3.2 Flow System

The flow system for this experiment is an adaptation of several previous researchers' work here at Stanford. Figure 3.3 shows the flow schema for this work. Squares with a T-x label denote pressure transducers. Circles with right angles inside denote three-way valves. Two-way valves are labeled to allow easier description of the layout in this report. Each major branch of the flow system will be discussed in detail in the next six sections. A listing of the major pieces of equipment is given in Appendix B, including their source of supply.

3.2.1 Injection System

The injection system consists of two LDC Analytical, Inc. model constaMetric 3200 pumps. Each pump has the capability to deliver 0.01 to 9.99 cm^3/min in 0.01 cm^3/min increments. The pumps use a dual plunger system that has been designed to provide constant fluid discharge rates at outlet pressures from 100-6000 psi. To use the pumps the user sets the desired discharge rate, the minimum allowable pressure, and

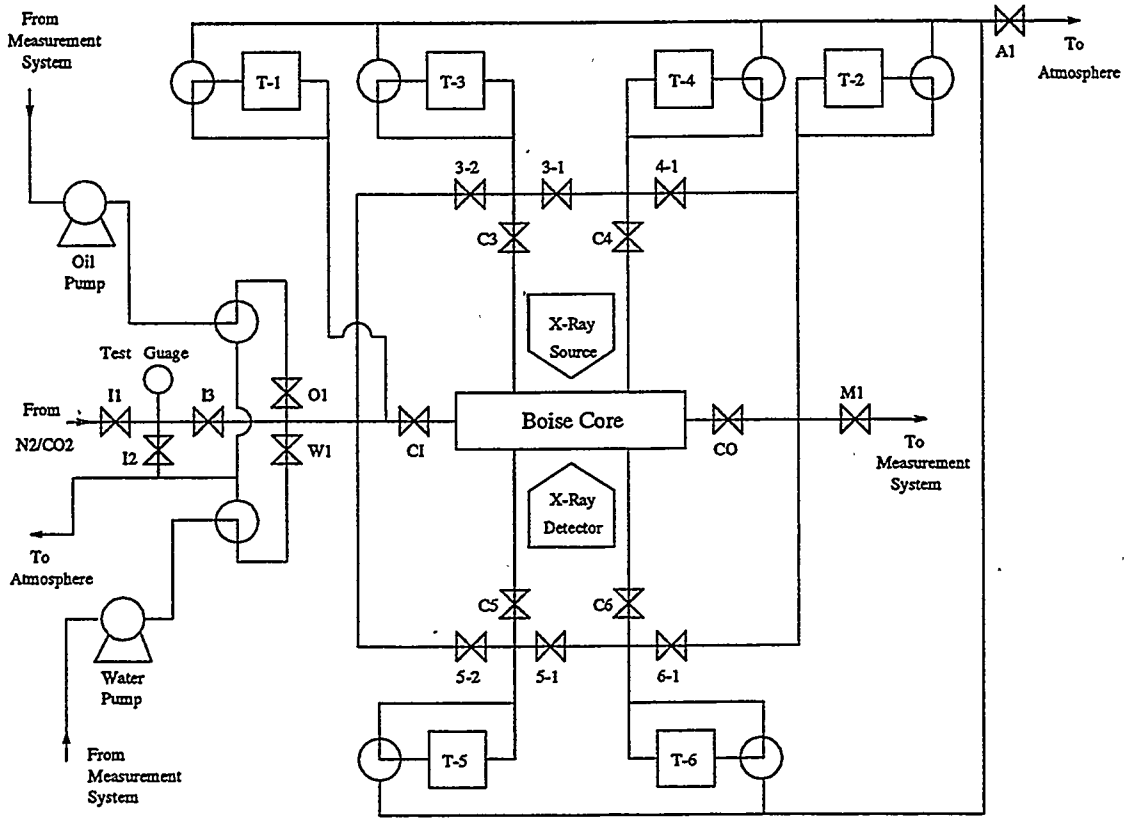

Figure 3.3: Experimental Flow Schematic.

the maximum allowable pressure. Plumbing downstream of the pumps allows mixing of the fluids being discharged by each pump. This setup allows injection pressure to be monitored with a test gauge and recirculation to measure pump output rates. This configuration also is a convenient way to use nitrogen in the calibration of the pressure transducers, or to use CO_2 to help in the saturation of the core. Pump inlet can be from an extra "make up" container or from the measured fluids being discharged from the core.

3.2.2 Distribution System

All piping used for the experiment was Paraflex 1/8 inch diameter, 500 psi working pressure plastic tubing with Swagelok fittings. The distribution of fluids throughout the experiment is controlled by Whitey B-43F2 ball valves. This system allows fluids to be directed to any port or combination of ports in the experiment. It can be directed to test the calibration of the pressure transducers, inject from one end and produce from the opposite end (the primary configuration), inject into one or more of the ports on the top and bottom of the core holder (which are normally used for monitoring pressures), or to bypass the core holder completely. The ability to direct fluids to any port in the experiment allows charging the core with fluids readily, testing various flow configurations, and cleaning the core more easily.

3.2.3 Production Measurement System

The production measurement system is an adaptation of a design first proposed by Ameri and Wang (1985) and modified by Qadeer (1994). Figure 3.4 shows the system.

The key element of the measurement system is the separator. It consists of two glass vessels, one inside the other. The inner vessel has an open bottom and a closed top. It hangs inside the outer vessel, suspended from an electronic balance by a hooked wire. Produced fluids enter this inner vessel and separate due to density differences. The lighter fluid (in this case, oil) rises and collects at the top of the inner vessel and the more dense fluid (water) exits from the bottom. The outer vessel is initially filled with water. When production begins, water from the inner vessel

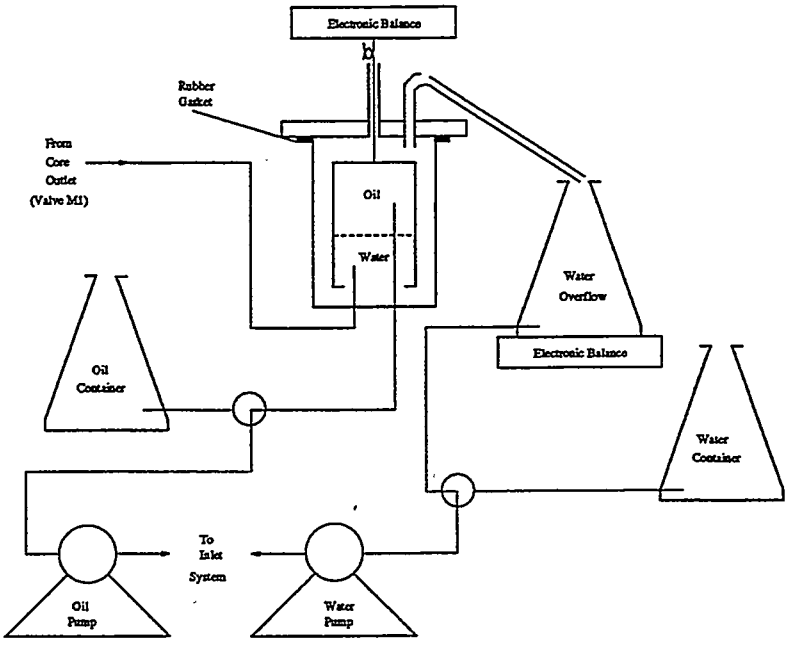

Figure 3.4: Production Measurement System.

is displaced into the outer vessel and in turn, displaces water from the outer vessel through the glass tube at the top. The glass tube has a hole in the top to break any siphon effect. Total liquid production is calculated by the amount of water that is collected in a beaker which sits on an electronic balance. The electronic balance attached to the inner vessel measures the buoyant weight of the vessel. From the weight change measured on this balance, oil production is calculated.

3.2.4 Pressure Measurement System

Pressure measurement for the experiment is accomplished through the use of six Celesco DP31 differential pressure transducers. Two of the transducers are connected to ports on the top of the core holder and two on the bottom. The ports are approximately 8 cm from each end. Two other transducers are connected to the inlet and outlet ends of the core holder. The negative side of each transducer is open to the atmosphere. This differs from the original work by Guzman and Aziz (1993). In their study, only the outlet end port had the negative side of the transducer open to the

atmosphere. The remaining ports had their negative side connected to the core outlet end. All the stainless steel diaphragms for the transducers are the 5 psi type. The Celesco transducers work in combination with carrier demodulators, either Celesco model CD10A, CD10D, or CD25A demodulators. The demodulators take the output from the transducers and produce a DC signal in the range -10 to +10 volts.

Calibration of the transducers is fairly straightforward and can be described best through example. Referring to Fig. 3.3, and focusing on the transducer labeled T-1, the three way valve is in the "loop back" position. Valves CI, 3-2 and 5-2 are closed and 5 psi of nitrogen pressure is applied by opening valves I1 and I3 and closing valves O1 and W1. Since the pressure is equally applied to both sides of the transducer, the transducer can be calibrated to zero pressure differential. Once the zero has been obtained, the three way valve is opened so that the negative side of the transducer is open to the atmosphere. The entire 5 psi of applied pressure is then being applied only to the positive side of the transducer. Since 5 psi diaphragms are being used, the output from the demodulator is adjusted to read +10 volts. This type of procedure is used on all pressure transducers.

3.2.5 Data Collection System

Output signals for the carrier demodulators can be collected by a set of Soltec Transducer Products, Inc. 1243 Chart Recorders, or the signals can be fed into an HP3497A data logger. If the data logger is used, the digital signal from the data logger is sent to an IBM compatible personal computer (PC) through a HP-IB interface card in the PC. Output signals from the two electronic balances are sent directly to serial communication ports in the PC.

3.2.6 Saturation Measurement System

Saturation measurement for this experiment is through the use of the Picker 1200SX Dual Energy CT Scanner. This scanner is a third generation medical scanner that has been modified for laboratory use. Table 3.1 gives a listing of various scanner settings used in this work. The interested reader is referred to the Picker 1200SX Operators Guide (1983) for further specifications on the system.

Table 3.1: Scanner settings.

Parameter	Setting
Field of View	30 cm
Image Matrix	512×512
Sampling	1024
Scan Rotation	398°
Scan Speed	3 sec
Slice Thickness	3 mm
Algorithm	14 (Spine)
Resolution	High
kV	100
mA	80
Focal Spot	Small
Anode Speed	Low
X-Ray Filter	C
Fast Process	Off
Dynamic Calibration	On
Dynamic Reference	On

Section 4

Experimental Results

Once the experiment had been designed and constructed, the equipment needed to be tested and evaluated for its ability to obtain meaningful results. This section describes and presents the results of experiments conducted in this effort.

4.1 Water Imbibition into a Dry Fractured Core

Guzman and Aziz (1993) presented a figure in their work which showed how the CT scanner can indicate unsaturated conditions within the rock matrix. For this study it was decided to evaluate how water imbibed into an unsaturated core. The first core that was used had the 1 mm fracture. Figure 4.1 shows the locations that were chosen for the CT scans. Two items prevented a regular sequence of scan locations. The first was that stainless steel fittings were used for the ports on the top and bottom of the core holder. These fittings caused artifacts and prevented scan locations from 70 mm to 85 mm and from 190 mm to 205 mm. These are distances measured from the inlet face. The second item that caused an irregular spacing of the scan locations was a large vug located 170 mm from the inlet face which we wanted to monitor throughout the experiment.

As noted in Section 3, the core holder had a gap corresponding to the width of the Viton gasket at both the inlet and outlet face of the core. At an injection rate of 1 cm^3/min, the injected water simply dribbled down the inside of the Plexiglas inlet

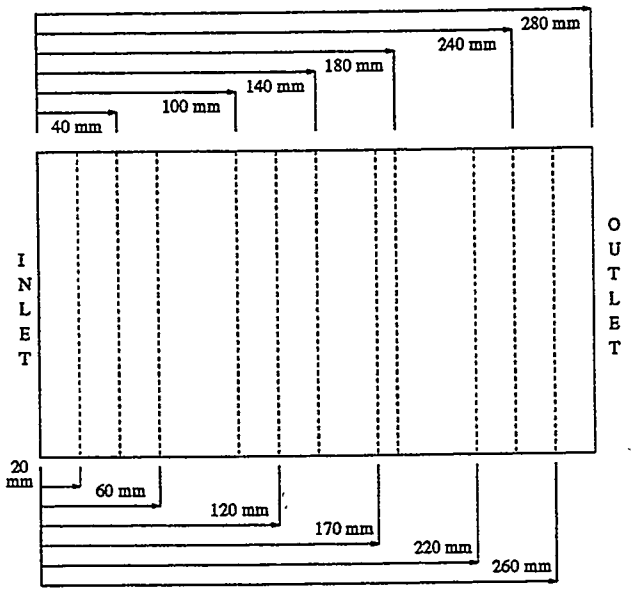

Figure 4.1: CT Scan Locations.

face plate and was imbibed into the bottom block. As the experiment progressed, the water began filling the gap between the Plexiglas plate and the core; however, it was very late in the experiment before the water got above the level of the fracture. The outlet condition was initially open to the atmosphere. After approximately 1.75 PV had been injected, the outlet was directed to the separation system and the injection rate was increased. Outlet pressure was 0.51 psi, while inlet pressure was 0.75 psi, at a flow rate of approximately 2 cm^3/min.

CT scans over time are shown in Fig. 4.2. This figure shows the fluid migration from approximately 0.03 pore volumes (PV) injected to 0.13 PV injected. Note that the scans indicate a hint that water is jumping across the fracture, at a position 60 mm from the inlet face after only 0.06 PV injected. There is a slight change in the lower right corner of the upper block. Figure 4.3 shows the 40 mm and 60 mm scans for 0.09 PV injected in slightly more detail. This figure has a different shading scheme than in Fig. 4.2. The reasons for the shading change and the methods for creating the figures are described in Appendix C. Of note in Fig. 4.3 is that there appears to be continuity across the fracture on the right edge of the blocks at these locations. The conclusion drawn from these figures is that the water crosses at these locations

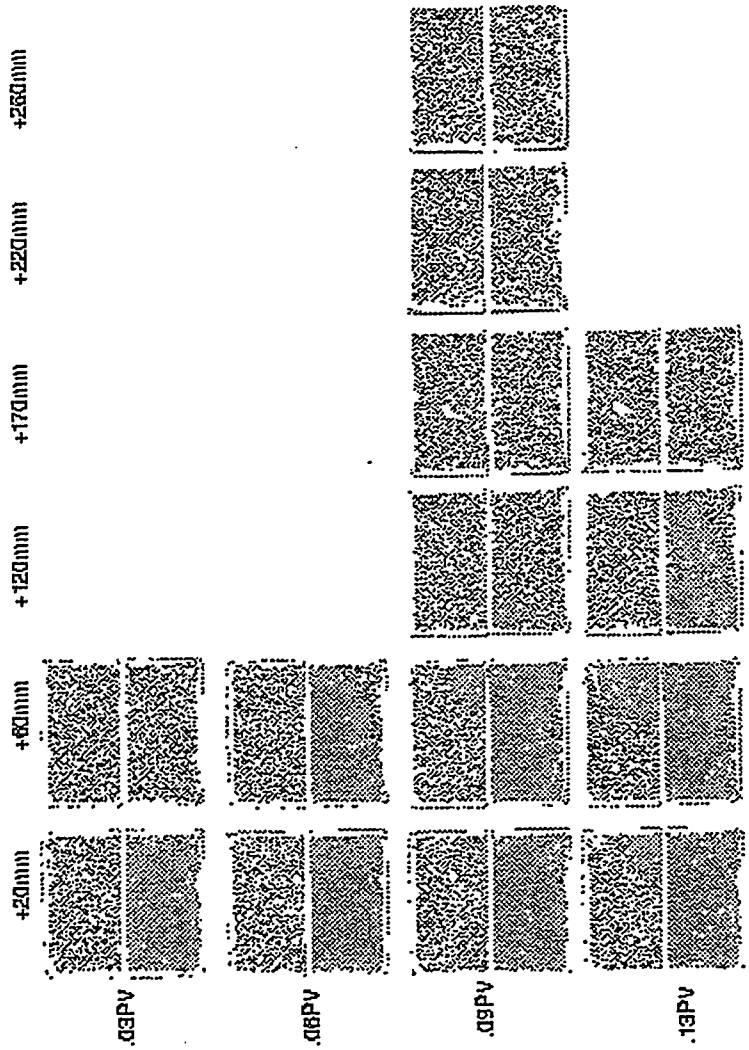

Figure 4.2: CT Scans at Early Times. Darker Shades Indicate Higher Water Saturation.

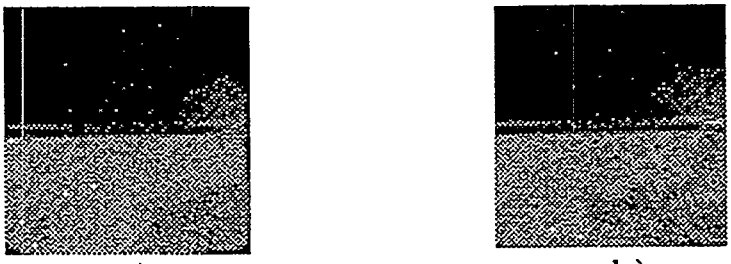

a.) b.)

Figure 4.3: CT Scan at a.)+40 mm and b.)+60 mm From Inlet End at 0.09 PV Injected. Lighter Shades Indicate Higher Water Saturation.

and then migrates towards the outlet face in the top and bottom blocks. The water also migrates back towards the inlet face in the top block. Presumably, this is due to capillary imbibition. Note also that water appears to be along the entire width of the fracture face on the top block in both the scan at 40 mm and the scan at 60 mm, but that the fracture seems to be filled with air (except on the right edge as noted above).

Figure 4.4 shows that, as the experiment progresses, the water continues to advance through the lower block at a faster rate than in the upper block. The water has found two streaks in the lower block which allow faster migration. One is adjacent to the fracture face in the center of the block. The other is in the lower right corner of the block. These can best be seen in the scans at 0.35 PV injected in the +220 mm location. Even though the water has advanced farther in the lower block, the upper block is achieving a higher saturation. The higher saturation is difficult to see on the figures, but can be seen when analyzing the raw CT numbers from the scans.

Water breaks through and begins collecting on the bottom of the outlet face plate at approximately 0.47 PV injected. Figure 4.5 shows that the upper block has water spread fairly evenly throughout, while the lower block still has areas not contacted. Figure 4.6 is the scan at 260 mm from the inlet face at the time of water breakthrough. It clearly shows areas where water has not contacted the rock pores.

The experiment was run over the course of four days. Approximately 4.26 PV of water passed through the core. Once the experiment was terminated, the valves

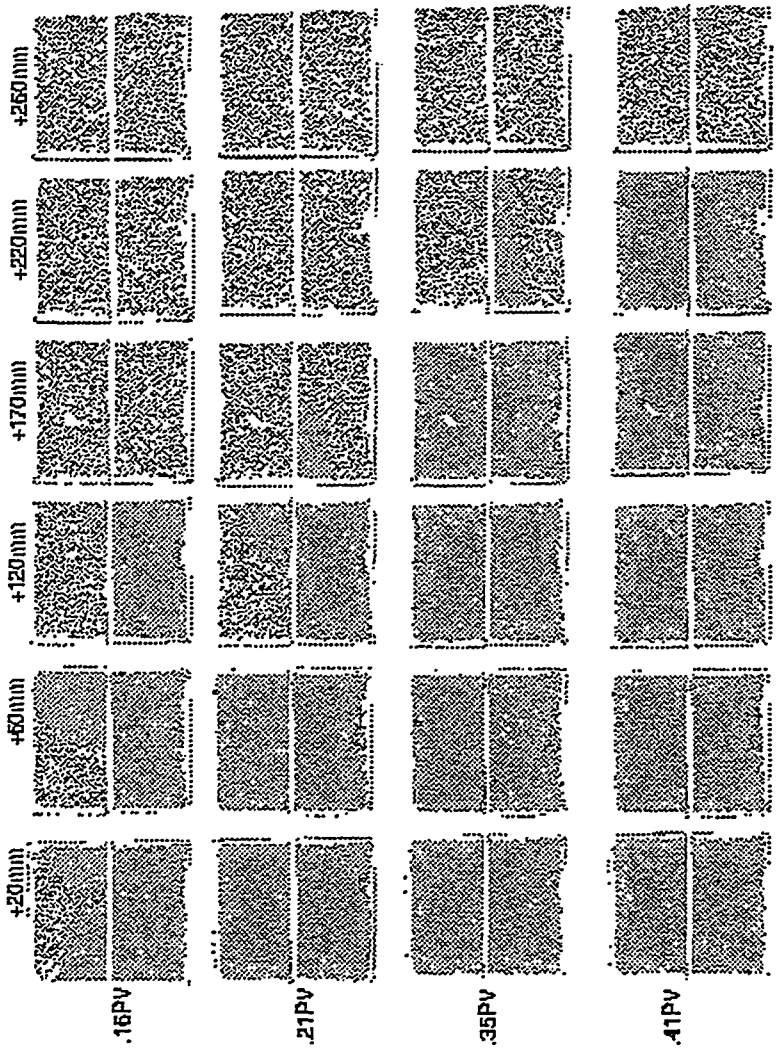

Figure 4.4: CT Scans as Experiment Progresses. Darker Shades Indicate Higher Water Saturation.

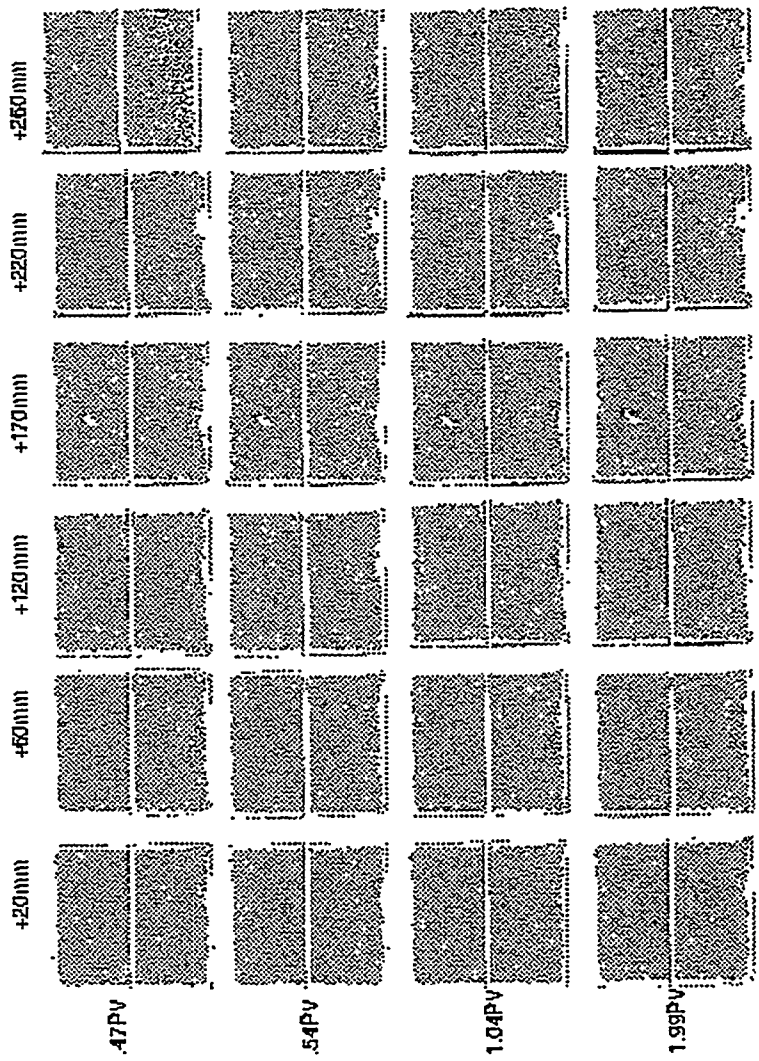

Figure 4.5: CT Scans at Water Breakthrough and Beyond. Darker Shades Indicate Higher Water Saturation.

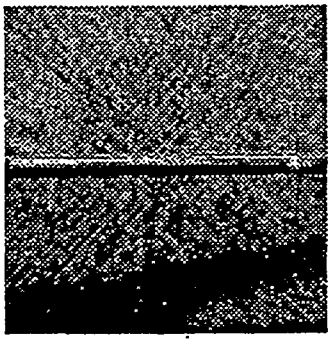

Figure 4.6: CT Scan at +260 mm From Inlet End at Breakthrough. Lighter Shades Indicate Higher Water Saturation.

leading to the core were closed and the core was allowed to sit for three months. The core was then scanned again. Figure 4.7 shows the scans at the end of the experiment, scans three months later, and the difference between them . The changes that occur seem to be most noticeable along the edges of blocks and the edges of the vug. These alterations could be caused by positioning errors, since the core holder was removed from the scanning table during the three month wait. A closer view of the scan at +170 mm from the inlet (the vug) is seen in Fig. 4.8. This view shows that the entire scan area has added water and that a pocket of air has formed on the top of the fracture adjacent to the top block. Note that the vug has filled considerably with water but that there continues to be a small area in the upper left side of the vug that contains air. This would suggest that, at least some of the changes seen in Fig. 4.7 are real, and not positioning differences. This figure also emphasizes the slow nature of the approach to equilibrium in porous media.

It is interesting to observe the changes that occur in the slice associated with the vug 170 mm from the inlet end. Figure 4.9 is the set of scans which shows these changes. In these figures, the lighter shades indicate higher water saturation values. The white spot in the upper right corner of the vug fills with water very early in the displacement process. Then more of the vug fills in as time goes on; however, the vug never becomes completely filled with water during the displacement.

One additional item on these experimental results is noteworthy. Withjack (1988) has shown that porosity can be calculated from the matrix of CT numbers obtained

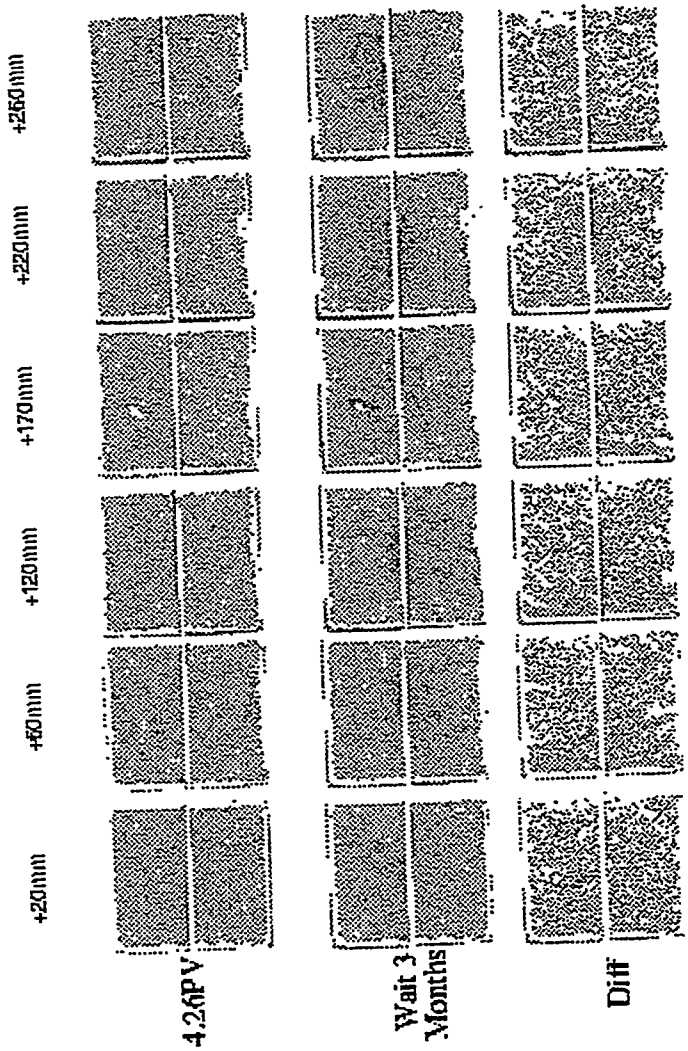

Figure 4.7: CT Scans Showing Fluid Movement Over 3 Months. Darker Shades Indicate Higher Water Saturation.

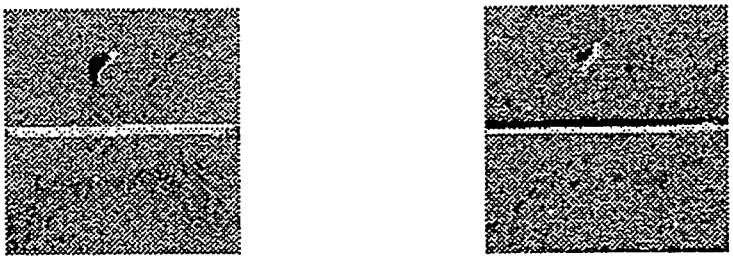

a.) b.)

Figure 4.8: CT Scans at +170 mm From Inlet End a.) at End of Displacement and b.) After 3 Month Wait. Lighter Shades Indicate Higher Water Saturation.

when scanning by using the equation:

$$\phi = \frac{CT_w - CT_d}{CT_{water} - CT_{air}} \tag{4.1}$$

where:

CT_w = the CT number for a water saturated core at a matrix location
CT_d = the CT number for a dry core at a matrix location
CT_{water} = the CT number for water
CT_{air} = the CT number for air

The CT number for water is 0, while the CT number for air is -1000.

Despite passing more than 4 PV of water through the core, the average value for "porosity" calculated from the scans at the end of the displacement experiment using Eqn. 4.1 was 14.35%. This differs from the average porosity measurements of 25.4% obtained by Guzman and Aziz (1993), 29.3% obtained by Sumnu (1995), and the 32% obtained by Sanyal (1972). Addition of CO_2 and injecting water into the pressure measurement ports raised the value calculated to an average of 20%. There continue to be areas (mainly in the lower block) that either have lower porosity or that have difficulty being saturated at the rates and pressures used in the experiment.

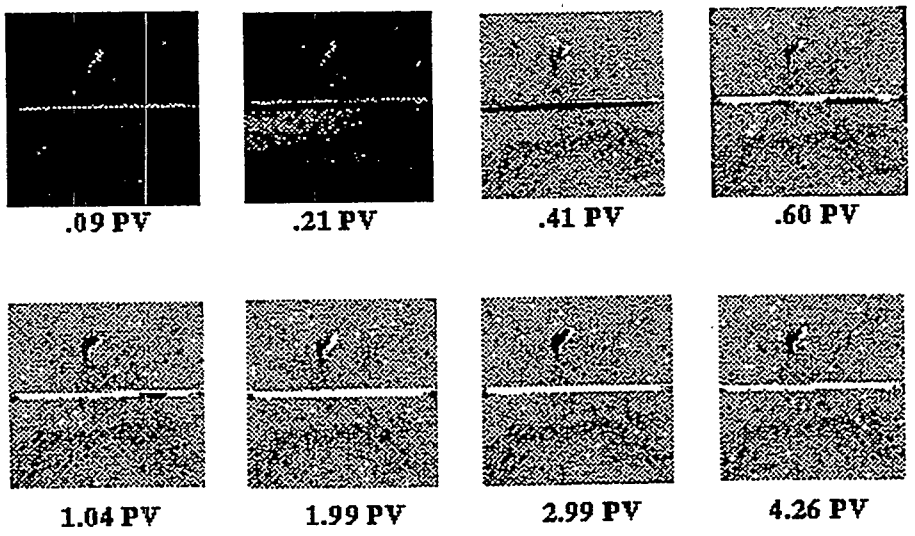

Figure 4.9: CT Scans at +170 mm From Inlet End Through Time. Lighter Shades Indicate Higher Water Saturation.

Section 5

Discussion and Recommendations

This report has presented the description of an apparatus to conduct experiments to investigate flow in fractured porous media. Preliminary experiments testing the equipment produced some interesting results. This section will evaluate the designed apparatus, suggest areas where improvements can be made, and provide insight into the results obtained thus far.

The experiments conducted thus far have shown that the system can obtain meaningful results in the effort to understand the physics of flow in fractured media. Flow in the experiment is across the blocks with gravity segregation possible at low rates. Thus, experiments can be run which mimic flow between wells (across the block) with water rising from below on one side. The flow configuration can be easily altered to accommodate other possible boundary conditions. Filter paper or fine grained sand could be used to fill the space between the Plexiglas plate and the core if a more even distribution inlet or outlet condition is desired. A tubing configuration could be devised similar to those in the Kazemi and Merrill (1979) study, if injection is to be limited to the fracture space. Experimental pressures have been as high as 16 psi and flow rates up to 10 cm^3/min have been recorded. The preliminary experiments have also shown areas in the rock which have lower permeability. These areas will need special attention when charging the core with oil, during displacement experiments, and also during cleaning operations. We would not have been aware of these problems if we had not had the useful additional information provided by the CT scanner.

As with any experimental apparatus, several areas needing improvement can be identified. Currently the pressure transducers are mounted on the edge of the top level of the cart being used for the experiment, while the three-way valves are mounted on a Plexiglas plate along an adjacent side of the cart. This allows easy access to the transducers for changing plates but it creates a web of lines which is difficult to decipher when lines are leaking or when changes to the system are needed. A taller cart would allow the transducers to be mounted on the Plexiglas plate next to the valves, and would still allow easy access should the plates need to be replaced. This would also considerably reduce the amount of tubing needed and also reduce the confusion caused by the existing lines.

To use the CT scanner to monitor the migration of fluids when the core is being charged with oil, or when the core is being cleaned, the stainless steel Swagelok fittings should be replaced with equivalent plastic fittings. Artifacts in the CT numbers will still occur due to the fittings, but these artifacts would be minor and would allow observation of saturation changes around the injection ports. These observations are not possible with the stainless steel fittings.

Several authors (Kazemi and Merrill (1979), Beckner (1990), Gilman, et al (1994)) have assumed that fracture capillary pressures are negligible. Others have shown experimentally that capillary continuity becomes important when gravity provides a driving force (Horie et al (1988), Firoozabadi and Hauge (1990), Labastie (1990), Firoozabadi and Markeset (1992a, 1992b)). Kazemi (1990) states his belief that capillary continuity is prevalent in the vertical direction and has suggested that, to reduce the number of equations to solve, fractured reservoir simulations should use the dual permeability formulation for the z direction, while the dual porosity formulation should be used for the x and y directions.

The CT scans shown in this report confirm that capillary continuity can occur in the vertical direction and also in the horizontal direction opposite to the pressure gradient. This continuity pulls fluid in the opposite direction of gravity. The continuity works in any direction depending on the relative strengths of the capillary and Darcy terms in the flow equations. Thus, the simulation engineer should evaluate the forces present in the system being simulated to decide which directions should be evaluated

by dual permeability equations, and which by dual porosity.

It should be noted that it remains unclear as to what has caused the continuity between blocks in this experiment. The most likely explanation is that fine grained material from cutting the end pieces may not have been thoroughly cleaned from the fracture. Some fine grained material was observed in the space between the rock and the Plexiglas end plates once the core had been filled with water. A repeat of this experiment should reveal whether this material caused the continuity across the fracture, or if there is some other mechanism.

Appendix A

Epoxy Specifications

Property	Specification
Resin System	Tap Plastics Marine Grade #314
Hardener	Tap Plastics Marine Grade #143
Resin/Hardener Ratio (by Volume)	2:1
Mixed Viscosity (cp)	780
Pot Life (minutes at 77° F, 25° C)	35–40
Recoat time (hours)	6.0–6.5
Recommended Minimum Use Temperature (° F)	40
Heat Distortion Temperature (° F)	110
Flexural Strength (psi)	10,500

APPENDIX A. EPOXY SPECIFICATIONS

Tensile Strength (psi)	7,000
Flexural Modulus (psi)	400,000
Tensile Modulus (psi)	360,000
Elongation %	6.0

Appendix B

List of Equipment

Equipment	Specification	Manufacturer or Distributor
Back pressure regulator	SD-91LW 400-25 psi	Grove Valve & Regulator Co. 6529 Hollis St. Oakland, CA 94608
Balance	PE1600	Mettler Instrument Corp. Princeton-Hightstown Road Hightstown, NJ 08520
	PE360	Mettler Instrument Corp. Princeton-Hightstown Road Hightstown, NJ 08520
Ball valve	Whitey B-43F2	Sunnyvale Valve & Fitting Co. 929 Weddell Court Sunnyvale, CA 94089
Connectors	Swagelock	Sunnyvale Valve & Fitting Co. 929 Weddell Court Sunnyvale, CA 94089

APPENDIX B. LIST OF EQUIPMENT

CT-Scanner	Picker 1200SX	Picker International, Inc 595 Miner Road Highland Heights, OH, 44143
Data Logger	HP3497A	Hewlett-Packard Co. P.O. Box 301 Loveland, CO 80537
Differential Pressure Transducer	DP31	Celesco Transducer Products, Inc. 7800 Deering Avenue Canoga Park,CA 91304
High performance liquid chromatography pump	constaMetric 3200	LCD Analytical, Inc. P.O. Box 10235 Riviera Beach, FL 33419
Personal computer	IBM compatible	
Relief valve	Nupro SS-RL3M4-F4	Sunnyvale Valve & Fitting Co. 929 Weddell Court Sunnyvale, CA 94089
Signal carrier or Demodulator	CD10A, CD10D CD25A	Celesco Transducer Products, Inc. 7800 Deering Avenue Canoga Park, CA 91304
Chart Recorder	1243	Soltec Transducer Products, Inc. 11684 Pendleton Street Sun Valley,CA 91352

APPENDIX B. LIST OF EQUIPMENT

Test gauge	Marshall Town 0-30 psi	Valin Corporation 209 Fair Oaks Ave. Sunnyvale, CA 94086
Three way ball valve	Whitey B-42XF2	Sunnyvale Valve & Fitting Co. 929 Weddell Court Sunnyvale, CA 94089

Appendix C

Graphic Files

For each CT scan taken there is a 512 × 512 matrix of CT numbers stored in a file. The data is formatted in such a way that it requires processing in order to create the graphics seen in Section 4. This processing is done in two ways.

The first method asks the user to input a CT number level and a CT number window. Any CT number that is larger than the level plus one half of the window is assigned a Tape Image File Format (TIFF) color value of 255. Any CT number that is smaller than the level minus one half the window is assigned a TIFF color value of 0. An output TIFF file is then created which scales the remaining CT numbers between 1 and 254. For these scans, a CT level of 1300 and a CT window of 325 was used. This means that CT numbers less that 1138 received color values of 0 and CT numbers greater than 1462 were given color values of 255.

To create Figs. 4.2, 4.4, 4.5, and 4.7, two files were required for each location at each time step shown. For each time step, the first data file is for the partially saturated scan and the second data file is for the dry scan at the same location. The dry scan TIFF file is then subtracted from the TIFF file from the time step using the software package NIF Image version 1.54 for the Macintosh. The resulting image was then copied into Microsoft PowerPoint version 3.0 for the Macintosh to create the montage of images for these figures.

This method was chosen for the figures which were showing fluid migration patterns for two reasons. The resulting greyscale images allow the reader to see bulk

fluid movement quite easily. The images are also easier to reproduce without losing picture quality.

The primary disadvantage in using this method is that it loses some of the most important data that we are trying to capture. Data in the fracture and in the vug have CT numbers that are below the value of 1138 in both the dry scans and in the partially saturated scans. All of the TIFF files contain zeros for the data values in the fracture and in the vug despite the fact that data changes do occur.

The second way to process the CT data uses a software package written for use with Stanford's Picker 1200SX scanner to access the CT numbers directly. This package uses script files written by the user to process the information. A script was created that reads in a partially saturated scan and a dry scan. It then subtracts the data in the dry scan from the data in the partially saturated scan and divides by 1000. This is, essentially Eqn. 4.1 with an unsaturated CT number substituting for the saturated value.

The script files in this processing package can use a variety of color palettes to create the resulting image. The color scheme chosen used shades of blue for low values, green for intermediate values and red for high values. A white color is used for off scale values on the high side, while a black color is used for off scale values on the low side.

A TIFF file is then created from the resulting matrix. For the scans in this report, a level of 0.15 and a window of 0.30 were chosen. This means that off scale values on the low side are registering negative values and are known to be data anomalies or artifacts. Off scale values on the high side are larger than 0.30.

This method was used in creating Figs. 4.3, 4.6, 4.8, and 4.9. The advantage of this method is that it shows subtle changes quite easily. It also uses and retains all of the data in the calculations. The biggest disadvantage to this method is the color scheme chosen. Use of this method for the fluid movement figures would have meant that Figs. 4.2 and 4.4 would contain a significant amount of black in the images. Our experience has been that these very dark images have a tendency to smudge and, in general, have poor image quality. Changes in the color scheme are in progress.

Nomenclature

A	Core cross sectional area
B	Formation Volume Factor
D	Depth
h	Reservoir thickness
K	Absolute permeability
k	Permeability
k_r	Relative permeability
L	Length
p	Pressure
Pc	Capillary pressure
q	Flow rate
S	Saturation
t	Time
T	Transmissibility
V	Volume

Greek

γ	Specific gravity
θ	Contact angle
μ	Viscosity
ρ	Density
σ	Interfacial tension or shape factor

NOMENCLATURE

ϕ	Porosity
τ	Matrix-Fracture transfer function

Subscripts

c	Capillary
D	Dimensionless
f	Fracture
m	Matrix
min	Minimum
max	Maximum
o	Oil
p	Phase
r	Relative
w	Water

Bibliography

[1] Aronofsky, J.S., Massé, L. and Natanson, S.G.: "A Model for the Mechanism of Oil Recovery from the Porous Matrix Due to Water Invasion in Fractured Reservoirs," *Trans.*, AIME (1958) **213**, 17–19.

[2] Ameri, H. and Wang, J.: "Effect of Temperature on Oil-Water Relative Permeability," SUPRI Heavy Oil Research Program, Eighth Annual Report, SUPRI TR–47, (April 1985), 11–24.

[3] Babadagli, T. and Ershaghi, I.: "Imbibition Assisted Two-Phase Flow in Natural Fractures," *SPE* 24044 presented at the Western Regional Meeting of the Society of Petroleum Engineers, Bakersfield, CA, March 30–April 1, 1992.

[4] Beckner, B.L.: *Improved Modeling of Imbibition Matrix/Fracture Fluid Transfer in Double Porosity Simulators*, PhD dissertation, Stanford University (July 1990).

[5] de Swaan, A.: "Theory of Waterflooding in Fractured Reservoirs," *SPEJ* (April 1978) 115–122.

[6] Firoozabadi, A. and Hauge, J.: "Capillary Pressure in Fractured Porous Media," *JPT* (June 1990) 784–791.

[7] Firoozabadi, A. and Markeset, T.: "An Experimental Study of Capillary and Gravity Crossflow in Fractured Porous Media," *SPE* 24918, presented at the 67th SPE Annual Technical Conference and Exhibition, Washington, D.C., October 4–7, 1992.

[8] Firoozabadi, A. and Markeset, T.: "An Experimental Study of Gas-Liquid Transmissibility in Fractured Porous Media," *SPE* 24919, presented at the 67th SPE Annual Technical Conference and Exhibition, Washington, D.C., October 4–7, 1992.

[9] Graham J.W. and Richardson, J.G.: "Theory and Application of Imbibition Phenomena in Recovery of Oil," *Trans.* AIME (1950) **216**, 377–381.

[10] Gilman, J.R., Bowzer, J.L. and Rothkopf, B.W.: "Application of Short-Radius Horizontal Boreholes in the Naturally Fractured Yates Field," *SPE* 28568, presented at the 69th SPE Annual Technical Conference and Exhibition, New Orleans, LA, September 25–28, 1994.

[11] Guzman, R. E. and Aziz, K.: *Design and Construction of an Experiment For Two-Phase Flow in Fractured Porous Media*, SUPRI TR–95, Stanford Petroleum Research Institute, Stanford, CA, (June 1993).

[12] Guzman, R. E. and Aziz, K.: "Fine Grid Simulation of Two-Phase Flow in Fractured Porous Media," *SPE* 24916, presented at the 67th SPE Annual Technical Conference and Exhibition, Washington, D.C., October 4–7, 1992.

[13] Horie, T., Firoozabadi, A. and Ishimoto, K.: "Capillary Continuity in Fractured Reservoirs," *SPE* 18282, presented at the 63rd SPE Annual Technical Conference and Exhibition, Houston, TX, October 2–5, 1988.

[14] Iffly, R., Rousselet, D. C., and Vermeulen, J. L.: "Fundamental Study of Imbibition in Fissured Oil Fields," *SPE* 4102 presented at the 47th Annual Meeting of the Society of Petroleum Engineers, San Antonio, TX, October 8–11, 1972.

[15] Kazemi, H. and Merrill, L. S.: "Numerical Simulation of Water Imbibition in Fractured Cores," *SPEJ* (June 1979) 175–182.

[16] Kazemi, H.: *Naturally Fractured Reservoirs*, Third International Forum on Reservoir Simulation, Baden, Austria (1990).

[17] Kazemi, H., Gilman, J.R. and Eisharkawy, A. M.: "Analytical and Numerical Solution of Oil Recovery From Fractured Reservoirs With Empirical Transfer Functions," *SPERE* (May 1992) 219–227.

[18] Kleppe, J. and Morse, R. A.: "Oil Production from Fractured Reservoirs by Water Displacement," *SPE* 5084 presented at the 49th Annual Meeting of the Society of Petroleum Engineers, Houston, TX, Oct.6–9, 1974.

[19] Kyte, J.R.: "A Centrifuge Method To Predict Matrix-Block Recovery in Fractured Reservoirs," *SPEJ* (June 1970), 164–170.

[20] Labastie, A.: "Capillary Continuity Between Blocks of a Fractured Reservoir," *SPE* 20515 presented at the 65th SPE Annual Technical Conference and Exhibition, New Orleans, LA, September 23–26, 1990.

[21] Lefebvre du Prey, E.: "Gravity and Capillarity Effects on Imbibition in Porous Media," *SPEJ* (June 1978) 195–206.

[22] Mattax, C. C. and Kyte, J. R.: "Imbibition Oil Recovery from Fractured, Water-Drive Reservoir," *SPEJ* (June 1962), 177–184.

[23] Parsons, R.W. and Chaney, P.R.: "Imbibition Model Studies on Water-Wet Carbonate Rocks," *SPEJ* (March 1966), 26–34.

[24] *Operator's Guide, Synerview 600s/1200SX, C850:F, REV1*, Picker International (January 1983).

[25] Qadeer, S.: *Techniques to Handle Limitations in Dynamic Relative Permeability Measurements*, PhD dissertation, Stanford University (in progress).

[26] Sanyal, S.K.: *The Effect of Temperature on Electrical Resistivity and Capillary Pressure Behavior of Porous Media*, PhD dissertation, Stanford University (December 1971).

[27] Sumnu, M.D.: *A Study of Steam Injection in Fractured Media*, PhD dissertation, Stanford University (November 1995).

[28] Withjack, E.M.: "Computed Tomography for Rock-Property Determination and Fluid-Flow Visualization," *SPEFE* (December 1988) 696–704.